

S11 USING MACHINE LEARNING APPROACHES FOR ENHANCING PREDICTABILITY OF SOUTHERN CALIFORNIA PRECIPITATION

Hannah Bao*

University of Maryland, College Park, College Park, Maryland

Linsey S. Passarella

Oak Ridge National Laboratory, Oak Ridge, Tennessee

Salil Mahajan

Oak Ridge National Laboratory, Oak Ridge, Tennessee

Maria J. Molina

University of Maryland, College Park, College Park, Maryland

1. INTRODUCTION

Extracting subseasonal-to-seasonal (S2S) predictability offered by low-frequency modes of variability, such as El Niño Southern Oscillation (ENSO), remains a challenge for Southern California precipitation. Current indices used to characterize ENSO and its teleconnections from the tropical Pacific, including the Niño 3.4 Index and ENSO Longitude Index, do not yield reliable subseasonal-to-seasonal predictability of Western United States precipitation (Passarella and Mahajan, 2023).

Passarella and Mahajan (2023) developed a multi-input multi-output autoencoder (MIMO-AE) that can extract the nonlinear co-variability patterns between tropical Pacific sea surface temperatures and Southern California precipitation anomalies on monthly time scales. They found that the index generated at the bottleneck layer of the MIMO-AE provides enhanced predictability of Southern California precipitation at a lead time of up to four months at the 95% confidence level, compared to the Niño 3.4 index and ELI (Passarella and Mahajan, 2023). We hypothesize that adding an additional input for North Pacific 500 mb geopotential height anomalies into the MIMO-AE network may provide enhanced predictability by better accounting for internal atmospheric variability (Myoung et al. 2018; Guirguis et al. 2020).

This ongoing study extends the work of Passarella and Mahajan (2023) to build a MIMO-AE network that can extract the nonlinear co-variability patterns between three input vectors: tropical Pacific sea surface temperature (TP-SST), Southern California precipitation (SC-PRECIP), and North Pacific geopotential height anomalies at the 500 mb (NP-Z500) pressure level. We aim to address the following questions:

- How can we use ML to maximize tropical-extratropical teleconnections as a source of S2S Southern California precipitation predictability?
- Can we improve upon the MIMO-AE designed by Passarella and Mahajan (2023) by adding a North Pacific Z500 anomaly input and generate an index better associated with Southern California precipitation?

2. DATA

We used 165 years (1850-2014) of monthly gridded historical simulation data at a spatial resolution of $1.0^\circ \times 1.0^\circ$ from the Energy Exascale Earth System Model version 1.0 (E3SMv1) large ensemble (E3SM Project, 2018). The MIMO-AE network was trained on the first 100 years (1850-1949) of the dataset for TP-SST, SC-PRECIP, and NP-Z500 anomalies and the remaining 65 years of data (1950-2014) was used to evaluate the predictive skill of the MIMO-AE index. Monthly anomalies were computed for TP-SST in the domain (20°N , to 20°S , 120°E to 70°W), SC-PRECIP in the domain (32°N to 35°N , 120°W to 114°W), and NP-Z500 in the domain (30°N to 65°N , 160°E to 140°W). The TP-SST and SC-PRECIP domains are consistent with those used by Passarella and Mahajan (2023). We used the North Pacific domain (30°N to 65°N , 160°E to 140°W) defined by Trenberth and Hurrell (1994) in their development of the North Pacific Index for measuring interannual-to-decadal atmospheric circulation variability. Monthly anomalies for each input variable were linearly detrended using least squares regression and scaled using a minimum-maximum scaler before training was performed.

3. METHODOLOGY

3.1 MIMO-AE

We use the MIMO-AE network to generate an index from which we can derive associated SC-PRECIP patterns. We chose a similar MIMO-AE architecture to the network designed by Passarella and Mahajan (2023), since this design was found to yield low reconstruction error and could explain at least 80% of Southern California precipitation variability for most domain grid points (Fig. 1b). Figure 2 illustrates our preliminary MIMO-AE network consisting of the three input (and output) vectors. The first dense hidden layer of the encoder contains 50 nodes and the second contains 10 nodes for each of the three separate inputs (Fig. 2). To add nonlinearity to the MIMO-AE reconstructions, we used the hyperbolic tangent activation (tanh) function for all hidden layers.

At the single-node bottleneck layer, we force the MIMO-AE network to learn the nonlinear relationships between the input variables and generate the MIMO-AE index. The MIMO-AE index is a one-dimensional vector over time, where each index value at a timestep t yields a different spatial pattern of the reconstructed inputs (Passarella and Mahajan, 2023). From the bottleneck

* Corresponding author address: Hannah Bao,
University of Maryland, College Park, College Park, MD 20740;
e-mail: hbao@terpmail.umd.edu

layer, we then pass the latent representation of the input data through the decoder of MIMO-AE to obtain reconstructions of the three original input fields. The decoder is symmetric in design to that of the encoder (Fig. 2).

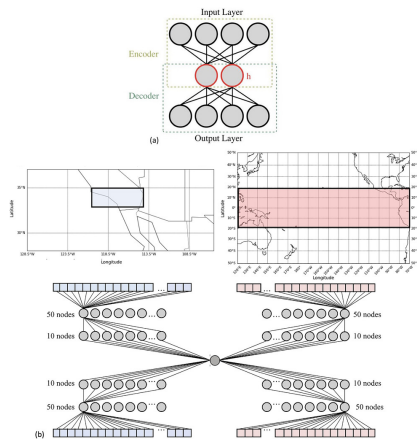


Figure 1. A simple autoencoder architecture (a), MIMO-AE architecture for two inputs and their reconstructions: tropical Pacific SST anomalies and Southern California precipitation anomalies (b). Figure reproduced from Passarella and Mahajan (2023).

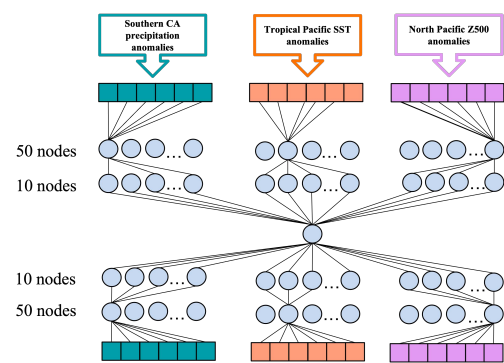


Figure 2. Three input-output MIMO-AE architecture consisting of tropical Pacific SST, Southern California precipitation, and additional North Pacific Z500 anomaly input-output.

The MIMO-AE was trained for 100 epochs with an Adam loss optimizer using TensorFlow. The training loss is calculated using a mean squared error between the MIMO-AE reconstructed data and original input data following a similar approach as Passarella and Mahajan (2023).

3.2. ASSESSING PREDICTABILITY PROVIDED BY THE MIMO-AE

We use LSTMs to further assess the relationship between the MIMO-AE index and SC-PRECIP patterns. LSTMs serve as our time series forecasting models to generate predicted values of the MIMO-AE index, regionally averaged SC-PRECIP, and other indices (e.g., Niño 3.4 and ELI) for the last 65 years of E3SM testing data (1950-2014). We chose the same LSTM architecture as Passarella and Mahajan (2023) consisting of 100 hidden nodes, since this design was

found to yield low training loss for all indices. We first assess the predictability of the MIMO-AE index itself. We build separate LSTM models for each of the time series of the indices (MIMO-AE index, Niño 3.4 index, and domain averaged SC-PRECIP) using the first 100 years (1850-1949) of E3SM data and trained the LSTMs for each of the forecast lead times from 0 to 12 months. The predictive skill of the LSTMs is subsequently tested on the last 65 years of E3SM data. We then compute the correlation between the LSTM predicted values of each index and the true value of each index.

Next, we pass LSTM-predicted MIMO-AE index values through the decoder of MIMO-AE to obtain SC-PRECIP spatio-temporal anomaly patterns. The SC-PRECIP anomaly patterns are domain averaged to obtain a time series and the correlation is computed between the predicted and true value of domain averaged SC-PRECIP. Both the MIMO-AE network and LSTM models were constructed in Python using Keras and TensorFlow Neural Network/Deep Learning libraries.

4. PRELIMINARY RESULTS

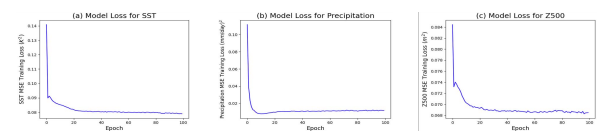


Figure 3. Training Losses for MIMO-AE over 100 epochs using scaled data for tropical Pacific SST (a); Southern California precipitation (b); and North Pacific Z500 anomalies (c).

In our preliminary investigation, we find that the MIMO-AE network constructed from the three input-output vectors yields low values of the mean squared error training loss function for each of the scale input data variables. The model converges to a loss of approximately 0.08 (Fig. 3a) for TP-SSTs, about 0.01 for SC-PRECIP (Fig. 3b), and about 0.068 for NP-Z500 (Fig. 3c).

We computed the R^2 values between the reconstructions from the MIMO-AE and original input data for the 100 years of training for SC-PRECIP (Fig. 4a), TP-SSTs (Fig. 4b), and NP-Z500 anomalies (Fig. 4c). The MIMO-AE explains about 60% of the variability of Southern California precipitation, about 4-12% of variability of Tropical Pacific SSTs, and approximately 4-8% of variability of North Pacific Z500 anomalies over most of the grid points in the respective spatial domains of each input variable. Our MIMO-AE explains smaller fractions of variability of SC-PRECIP and TP-SSTs compared to the two input-output MIMO-AE developed by Passarella and Mahajan (2023), which was found to explain over 80% of the variability of SC-PRECIP and up to 20% of the variability of TP-SSTs. In the future, we intend to further explore different network designs that can explain larger fractions of SC-PRECIP variability.

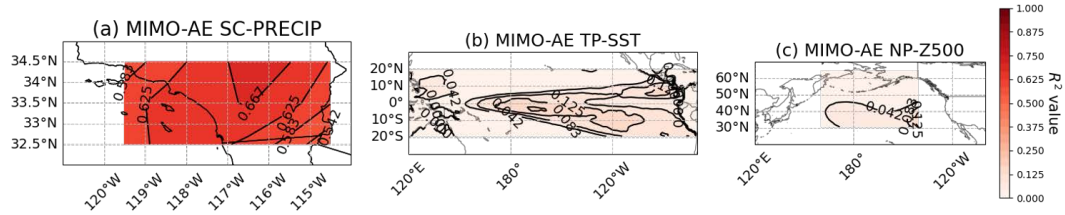


Figure 4. R^2 values between MIMO-AE reconstructed and original input data for SC-PRECIP (a); TP-SST (b); and NP-Z500 anomalies (c).

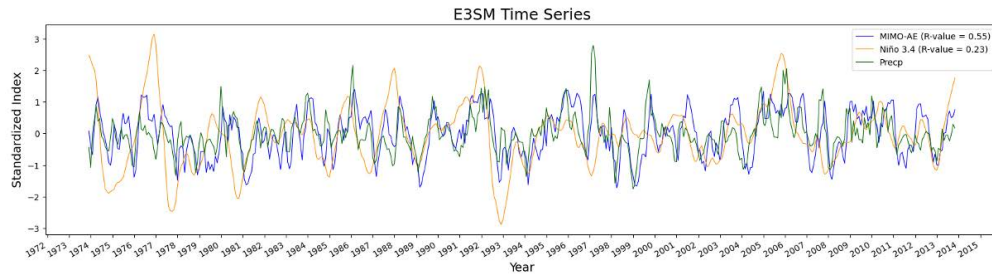


Figure 5. Three-month moving average of the standardized time series of MIMO-AE index (blue), Niño 3.4 index (orange), and domain average SC-PRECIP (green) for a segment (last 40 years: 1974-2013) of the 65 years of E3SM historical simulation testing data.

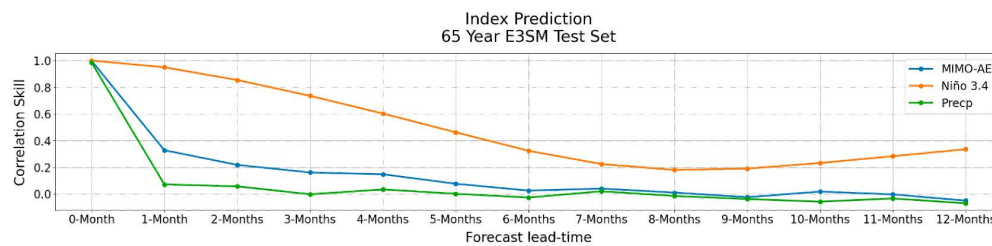


Figure 6. Correlation skill between LSTM-predicted values and true values of MIMO-AE index (blue), Niño 3.4 index (orange), and domain averaged SC-PRECIP at forecast lead times of 0 to 12 months for E3SM testing data.

Figure 5 shows the three-month moving average of the standardized time series of the MIMO-AE index, and Niño 3.4 index, and regionally averaged SC-PRECIP for a segment (last 40 years: 1974-2013) of the 65 years of E3SM testing data. The Pearson's correlation coefficients of each time series against domain-averaged SC-PRECIP were also computed for the smoothed data (Fig. 5). The correlation between SC-PRECIP and the MIMO-AE index (0.55) is higher than between SC-PRECIP and the Niño 3.4 index (0.23), given that we used SC-PRECIP data to generate the MIMO-AE index and our MIMO-AE can explain up to 60% of SC-PRECIP variability.

The predictability of the MIMO-AE index itself, along with the predictability of the Niño 3.4 index and domain-averaged SC-PRECIP, at lead times of 0 to 12 months are shown in Figure 6. The MIMO-AE index shows stronger correlation skill than domain-averaged SC-PRECIP for lead times between 1 month to 6 months (Fig. 6). The MIMO-AE index exhibits weaker correlation skill than the Niño 3.4 index at all lead times longer than 1 month. This is similar to the results from Passarella and Mahajan (2023), which also found that the MIMO-AE index showed lower correlation skill than the Niño 3.4 index at all lead times exceeding 1 month. Passarella and Mahajan (2023) suggest that noisy precipitation may be a possible factor in lowering the correlation between the LSTM-predicted values of MIMO-AE index with the true values of the MIMO-AE index.

5. SUMMARY

Preliminary results show that the MIMO-AE index generated from three input fields (TP-SST, SC-PRECIP, and NP-Z500 anomalies) exhibits weak correlation skill between LSTM-predicted values of the index for lead times longer than 1 month. Our MIMO-AE network explains the largest fractions of variability for the SC-PRECIP input compared to the TP-SST and NP-Z500 inputs. However, the three-input-output MIMO-AE overall explains a lower fraction of SC-PRECIP variability compared to the two input-output MIMO-AE by Passarella and Mahajan (2023).

6. FUTURE WORK

Ongoing work aims to evaluate the correlation skill of domain-averaged SC-PRECIP patterns constructed from LSTM-predicted values of the MIMO-AE index and true domain-averaged SC-PRECIP. We also intend to further explore hyperparameter tuning to obtain the optimal network design for the MIMO-AE network which yields low training loss, while explaining larger fractions of Southern California precipitation variability. This may involve using the KerasTuner framework to find the optimal set of hyperparameters while training the MIMO-AE as well as experimenting with varying number of nodes, hidden layers, and testing other activation functions.

Additionally, we aim to use transfer learning to train the MIMO-AE on a combination of simulation and observational data, as this approach was shown by Passarella and Mahajan (2023) to provide enhanced predictability of Southern California precipitation on the S2S scale compared to training the MIMO-AE solely on simulation data.

7. ACKNOWLEDGEMENTS

This research used resources of the Oak Ridge Leadership Computing Facility at the Oak Ridge National Laboratory, which is supported by the Office of Science of the U.S. Department of Energy under Contract No. DE-AC05-00OR22725.

8. REFERENCES

- E3SM Project, 2018: Energy Exascale Earth System Model v1.0. U.S. Department of Energy, <https://doi.org/10.11578/E3SM/dc.20180418.36>.
- Guirguis, K., Gershunov, A., DeFlorio, M. J., Shulgina, T., Delle Monache, L., Subramanian, A. C., Corringham, T. W., and F. M. Ralph, 2020: Four atmospheric circulation regimes over the North Pacific and their relationship to California precipitation on daily to seasonal timescales. *Geophys. Res. Lett.*, **47**, e2020GL087609, <https://doi.org/10.1029/2020GL087609>.
- Myoung, B., Yeh, S. W., Kim, J., and M. C. Kafatos, 2018: Impacts of Pacific SSTs on atmospheric circulations leading to California winter precipitation variability: A diagnostic modeling. *Atmosphere*, **9**, 455, <https://doi.org/10.3390/atmos9110455>.
- Passarella, L. S. and S. Mahajan, 2023: Assessing tropical Pacific-induced predictability of Southern California precipitation using a novel multi-input-multi-output autoencoder. *Artif. Intell. Earth Syst.*, **2**, e230003, <https://doi.org/10.1175/AIES-D-23-0003.1>.
- Trenberth, K. E. and J. W. Hurrell, 1994: Decadal atmosphere-ocean variations in the Pacific. *Climate Dyn.*, **9**, 303–319, <https://doi.org/10.1007/BF00204745>.